# DIFFERENCES OF ULTRASOUND PROPAGATION IN TISSUE AND TISSUE MIMICKING MATERIALS

Jaroslav Satrapa[1] and Ivan Zuna[2]

[1]TCC, A-4850 Timelkam, Lenaustr. 10

[2]DKFZ, D-6912 Heidelberg,. Im Neuenheimer Feld 280

## INTRODUCTION

The ultrasound images taken on homogeneous and isotropic tissue mimicking phantoms cannot be directly compared to the images taken from inhomogeneous and anisotropic tissue. For this purpose special comparison and measuring methods for the recognition and quantitative enhancement of the propagation phenomena in inhomogeneous media were developed. Propagation phenomena appear in many cases as special attenuation issues or as characteristic frequency dependent back scattering. By severe speed of sound inhomogeneities appears serious reduction of image contrast accompanied by reverberations and multiple scattering.

It is known that causality between tissue structure and propagation parameters, respectively image statistical parameters, are especially important. The study of these causalities is associated with difficulties, if the parameters of the reference tissue mimicking objects, are not precisely known.

Besides the methods for measuring attenuation, speed of sound and back scattering, the new methods arc developed for estimating the contrast reduction, anisotropy and inhomogeneities for tissue and tissue mimicking materials. The new materials are proposed as propagation reference objects. The methods are supported with mathematic models and simulations. Some applications of novel methods in vivo will be illustrated.

The ultrasound propagation is characterized by very complex interaction of ultrasound waves and tissue structure. The complex interaction may be described by physical parameters of the scanner, as well as by propagation parameters of the tissue. Both parameter groups influence the generation of the B-image. The determination of‘ scanner parameters is the basic condition for the estimation of propagation parameters and tissue characterization Mostly the interrogating tissue is not in immediate connection with the scanner. The tissue, skin, fat or muscles. Between scanner and object, influences the image appearance in some cases essentially. Generally, there is a certain ***tissue “stand off”*** **w**ith different propagation properties. In many cases this “stand of” is homogeneous and can he compared with many tissue mimicking materials, however, some abdominal walls and breasts show full complexity of nonhomogeneous propagation coming from irregular interlacing of fat and collagen.

The nonhomogeneities are in the speed of sound and attenuation and cause the phase aberrations and additional generation of side lobes. In a strong nonhomogeneous environment the reverberation and multiple scattering is observed. It blurs the image and reduces the image contrast. In many cases, only reduced contrast is visible in B-image.

***Acoustical Imaging,*** *VoI.* 22, Edited by P. Tortoli
and L. Masotti, Plenum Press, New York, 1996

In the effort to improve the B-scanners diagnostic efficiency, the special phantoms or reference objects are developed as a tool for estimation of unknown scanner parameters and quantification of attenuation, backscattering, reverberation and contrast reduction.

The reference object image, delivers the parameters for gray level histogram normalization and gray level calibration. Normalization is equivalent to the restoration of statistical parameters of the first order. The image correction is still object of research, in the sense of essentially improving of contrast and elimination of reverberation.

In order to estimate the system parameters accurately, the phantom materials parameters such as speed of sound, attenuation and back scattering with their characteristic temperature and frequency dependencies must be known. The parameters of homogeneity and anisotropy help also for the estimation of propagation parameters.

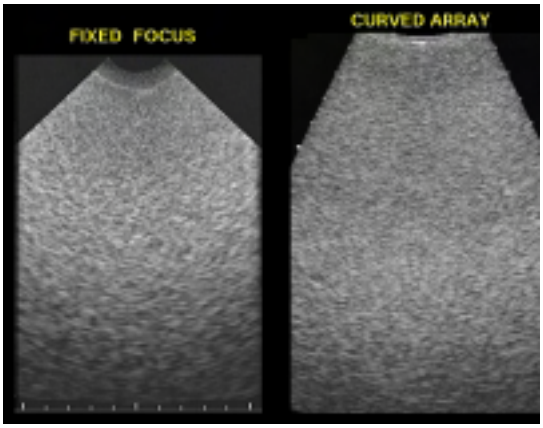


Fig.1 - There is the noticeable difference in speckle pattern for die Same object and different scanners

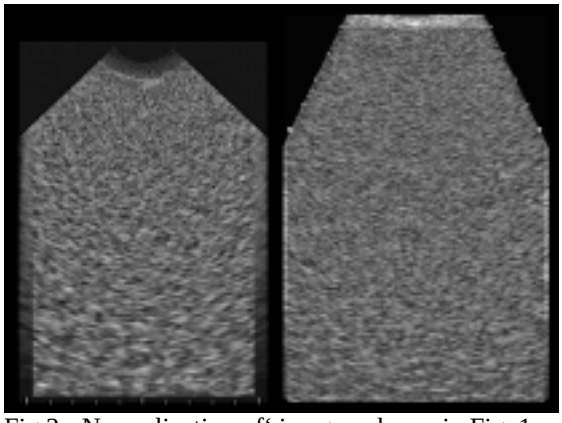

Fig.2 - Normalization of‘ images, shown in Fig. 1, using the equalization of *mean* and *standard deviation* for all depths.

The scanner is characterized with parameters as axial, lateral and elevation resolution. The better alternative to these parameters is the detectability of small cysts. The cysts detectability corresponds substantially to die contrast resolution as a detectability for focal lesions. All three aspects of resolution, respectively axial, lateral and elevations resolution are involved in the mentioned cysts detectability. The 8-imaging is accompanied with large depth variations of cysts detectability. Fortunately the cysts detectability is directly measurable under specific conditions using phantoms with spherical or cylindrical voids acoustically equivalent to small cysts.

## BASIC OBSERVATIONS OF PROPAGATION PHENOMENA

The propagation phenomena may be directly observed by the B-scanner and by suitable objects immersed in water. A convenient way to show die propagations phenomena is a sequence of examples.

Fig. 1 shows the B-images of artificial foam immersed in water with a fixed focus scanner and a curved array scanner.

Although both images represent the same object, there is a fundamental difference in the speckle pattern. If the nonlinear distortion of the local dynamic range is eliminated, the histogram analysis shows that die gray levels of both images follow the Rayleigh distribution.

The gray level distribution is independent from the position in the image and is the same for the near field, far field or focus. The shape of the speckle corn characterizes the system resolution, but the system resolution cannot be unambiguously estimated from the shape of the speckle corn or from the autocorrelation function.

The aprior knowledge about the Rayleigh distribution is used for gray level calibration. It means that the histogram of the homogeneous foam image may be normalized using PC and frame grabber and equalized in mean and standard deviation for all depth, Fig.2.

What supplementary information can be extracted from the B-image of the foam? The optical microscope image of the foam shows the spatial lattice as short threads in space, mutually connected in knots. The position of lattice cells in space is random and thickness of the short fibers (fibrils) is almost equal. The number of fibers per volume unit and their orientation change across the space. It may be expected that interference of ultrasound waves and described lattice structure will have the consequence in some resonance and aliasing effects normally not noticeable in the B-image.

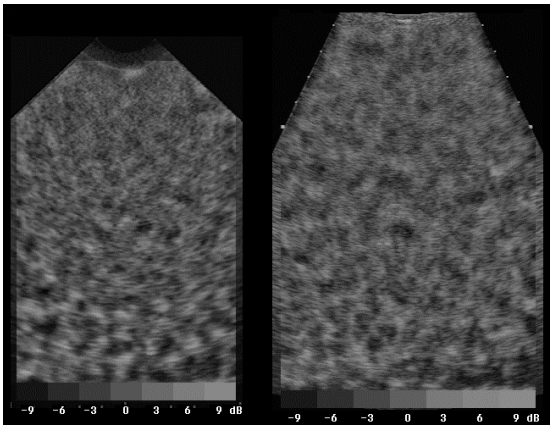


Fig.3 - Enhancement of normalized images shown in Fig. 2, by weighting and summing (WS) processing.

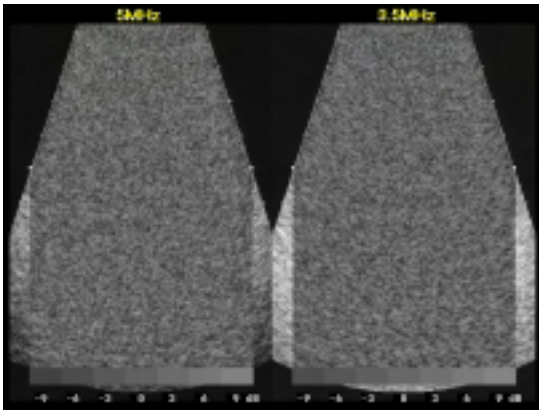

Fig.4 - The normalized images, taken at the same B-plane with frequency switchable scanner, do not show obvious differences.

In the homogeneous artificial foam B-image, the strong changes of scatterer density, which causes large deviation from Rayleigh distributions, cannot be observed. Only the weak differences in gray levels, like darker and brighter areas may be observed. The B-image decomposed in several spatial frequency bands and composed the frequency bands back by *Weighting* and *Summing* (WS) processing; let us see these weak differences better, Fig.3.

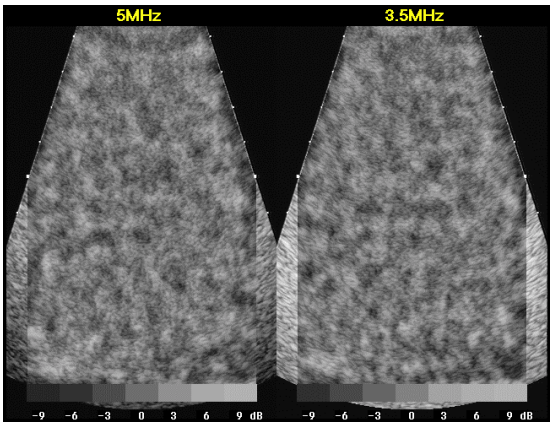


Fig.5 - The same images, shown in Fig 4, processed by WS present clearly the frequency dependent areas of backscattering.

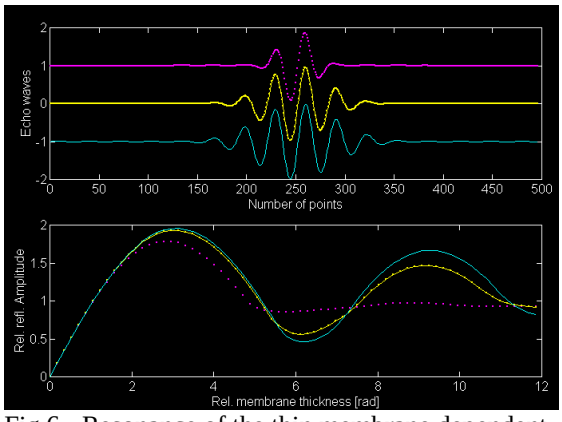


Fig.6 - Resonance of the thin membrane dependent from, the echo shape and membrane thickness.

The processed image shows indeed patterns of different gray level areas corresponding to different scatterer densities or aliasing effects due to the anisotropy in the lattice structure.

Which in both effects is responsible for areas, looking like lesions or specific texture, can be found by insonification of the same B-plane by different scanner frequency bands. With frequency switchable scanners, die normalized images do not show obviously the differences Fig.4. The same images processed by WS shows clearly the frequency dependent areas of backscattering, Fig. 5. Bark areas in both images at the same places indicate the lower scatterer density.

Due to the scatterer fiber shape of he presented foam structure it has the typical frequency dependent backscattering, increasing with 6 db/octave or 20dB/decade, corresponding to the frequency dependency of single fiber or thin membrane. The membrane shows the typical frequency dependency behavior with resonance effect by frequency, corresponding to $\lambda/4$ of membrane thickness, Fig.6.

## PROPAGATION IN LIVING TISSUE

In comparison with foam immersed in water, the living tissue is characterized by inhomogeneities given by anatomical structure or caused by a pathological process. In the case of a diffused disease, the tissue structure will be changed, but the homogeneous character is maintained. The tissue frequency dependent backscattering is strongly structure dependent and may differ from values found in foam and liver.

The inhomogeneities and changes of tissue structure may be observed in B-images but not measured with available diagnostic instruments. Deficient conception of propagation in tissue may be improved by:

- computer modeling of propagation in tissue and
- experimental measurement of propagation phenomena

The most popular method of modeling by computer is the multidimensional convolution model successfully applicable for non-attenuating and non-reverberating media. The convolution model that much more simplifies the propagation and many essentially important propagation phenomena cannot be studied on such model.

More suitable is the RAY-tracing model, primarily used for sliced structures and plane waves. The RAY model applied, on general structures, can be very intensive for computing and time consuming. Due to such shortcomings it finds the application only in special cases.

Experimental proof is unavoidable in any case for models and simulations. The comparison between tissue and reference object is not limited in any sense, but needs the careful choice of experimental set up, taking in to account that a prior knowledge and possible large set of quasi artifactual appearances and propagation explicitness.

Let us see the basic observations and the explicitness of propagation.

Fig.7 shows the typical sound amplification“ and ‘shadowing“ effected by gap (opening) and bar (obstruct). The propagation in non-homogeneous tissue in the sense of attenuation has randomly distributed “gap and bars‘.

For experimental purposes the regular array of steel bars with diameters of 0.5 mm and 1 mm distance put at die front of the transducer, Fig.8, generates the grating lobes and reduces the contrast of image. Images show the phantom voids with 5mm diameter and the image of the same object influenced by an array of steel bars.

The slice of animal fat put on the front of a transducer evokes also contrast reduction, Fig.9. The “random array“ of fat and collagen with interlaced muscles produces the side lobes caused from inhomogeneities in attenuation and in speed of sound.

It is coming primarily from the acoustical difference between fat and collagen. Strong reverberations and multiple scattering can be observed as diminishing brightness behind the slice of fat immersed in water, Fig.10.

In order to correct exactly the image, the correction of ***amplitude and phase*** for any RAY must be accomplished and for all ranges of images separately. It is not known how to correct the complex reverberations.

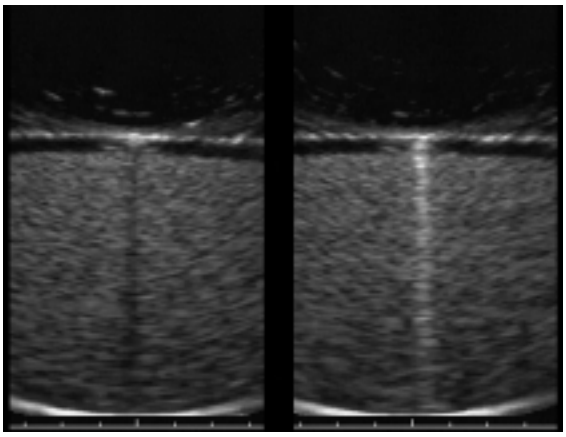

Fig.7 - The typical „shadowing“ (a) and “sound amplification“ (b), effected by gap (opening) and bar (obstruct), are basic appearances of propagation in attenuating and non-homogeneous media.

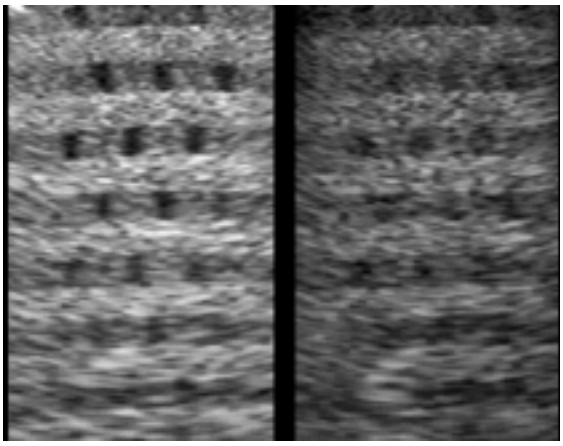

Fig.8 - Regular array of steel bars put at the front of the transducer, reduce the contrast of image; a) Image of small cylindrical voids included in phantom; b) Image taken with the same phantom, with the steel bars array, put at the front of the transducer.

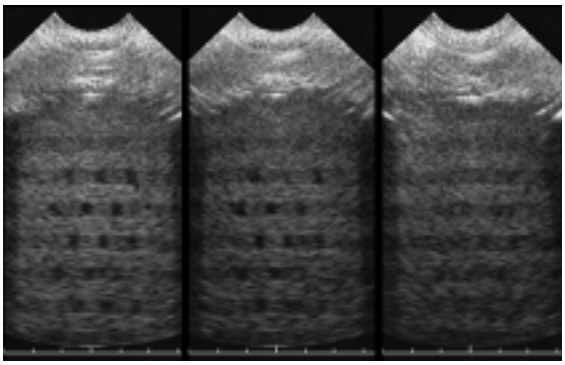

Fig.9 - The slice of animal fat put on the front of the transducer evokes contrast reduction. The “random array” of fat and collagen with interlaced muscles produces the side lobes caused from inhomogeneities in attenuation and in speed of sound. Images show the phantom with cylindrical voids, with three different positions of animal fat slice used as stand off.

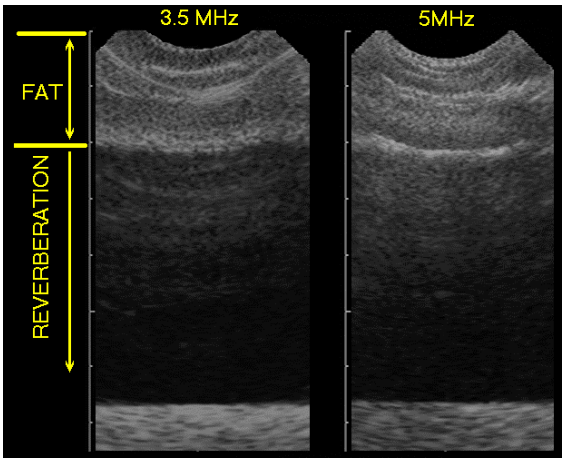


Fig.10 - Strong reverberations and multiple scattering can be observed as diminishing behind the slice of animal fat immersed in water.

## PROPAGATION IN OTHER ARTIFICIAL MEDIA

The graphite powder in gelatin shows a similar attenuation characteristic as foam. Only the back scattering follows other frequency dependence other then it is found in foam or liver. The reason for such behavior is relative high acoustic impedance of graphite (4 MRayl) compared to collagen (1.6 MRayl) and polyurethane (1.7 MRayl), and small dimensions of graphite corn (40μ). In order to mimic the liver frequency dependency of

backscattering, the glass beads are usually added to the graphite corn. Glass beads, as spherical targets do not show the typical anisotropy effect as some tissues or foam.

With rubber based phantoms it was possible to avoid the water desiccation. The main disadvantage of polyurethane rubber is the low speed of sound from 1450 m/s. The attenuation presents itself mainly as absorption. It is not know how to produce the typical tissue frequency dependent back scattering in such absorbing media.

## PRACTICAL WAYS OF B-IMAGE PROCESSING

The correction of the B-image may be calculated by using the data from a reference object image. The condition for image pixels correction is the small difference between the attenuation of the reference object and the tissue. Taking this condition in to account, the diffraction error will be minimized. The new image pixel value will be given by the shown expression:

$$p_n(j,i) = \mu_n + \sigma_n * [\, p_o(j,i) - \mu_o(j,i)] / \sigma_o(j,i) \quad (1)$$

where

$\mathbf{p_n}$ = new pixel value
$\boldsymbol{\mu_n}$ = new mean
$\boldsymbol{\sigma_n}$ = new standard deviation
$\mathbf{p_o}$ = pixel of original object image
$\boldsymbol{\mu_o}$ = mean of reference object image
$\boldsymbol{\sigma_o}$ = standard deviation of reference object Image

The $\mu_o(j,i)$ and $\sigma_o(j,i)$ may be prepared previously as moving averages in 2D look up tables. The result in general approach is 2D look up table LUTj,i

$$p_n(j,i) = LUTj,i\, [\, p_o(j,i)] \quad (2)$$

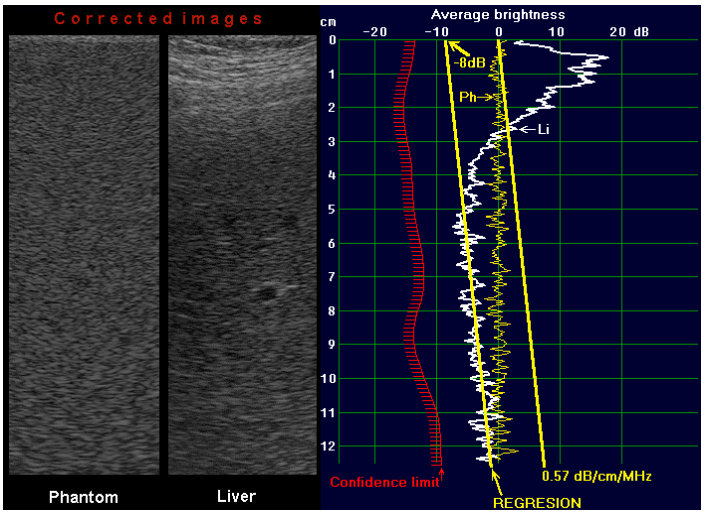


Fig. 11 - Normalized images of reference object (phantom) and liver. The reverberation of abdominal wall is very strong and progresses deep in the liver parenchyma diminishing at the depth of 4cm. The averages of brightness, presented as curves from reference object and liver, show clearly the reverberations range of abdominal wall. The brightness regression line for liver delivers the estimation for backscattering and attenuation of liver.

Fig. 11 shows already the normalized reference object and liver image. From the normalized images follow the estimation of liver attenuation and back-scattering. The backscattering and reverberation of abdominal wall is very strong and progresses deep in the liver parenchyma. By TGC adjustment, the mostly strong abdominal wall back-scattering, will be adjusted unconsciously and wrongly away. The image normalization recovers this wrong adjustment and gives the information and impression about abdominal backscattering and quasi-hidden reverberation. The possible reduction of contrast by the abdominal wall is already shown.

Typical pathologic liver appearance is accumulation of fat and collagen as fibrosis. Eight cases of liver interrogation show the spreading of attenuation and backscattering, Fig. 12. The normalization of B-images

and WS processing cannot improve the detectability of small cysts. For this reason it is of serious significance to find out, for any scanner, the cyst detectability for different cyst sizes and usable scanning depths. The best illustration of such measurements presents the phantom with cylindrical voids taken with 3D scanner in sequence of C-images, Fig.13.

A special problem is the estimation of contrast reduction due to the tissue inhomogeneities.

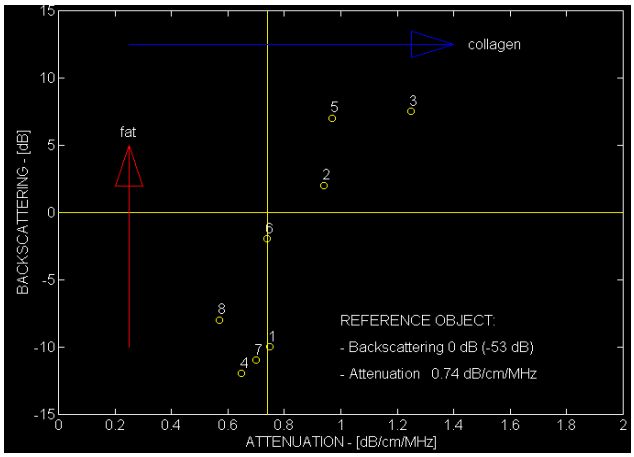


Fig.12 - Typical pathologic liver appearance is accumulation of fat and collagen as fibrosis. Eight cases of liver interrogation show the spreading of attenuation and backscattering.

A unique possibility for the direct measurement of contrast reduction reveals the breast. The breast when pressed, as usual in mammography, creates the shape like “stand off” and the contrast reduction may be estimated in the same way as shown with animal fat Fig.14 and 15. The phantom is provided with nylon threads and cylindrical voids. Only the nylon threads are visible and the voids disappeared. The nylon threads are specular reflectors and behave obviously differently than voids.

The contrast and contrast-reduction can be treated quantitatively using normalized images. Haralick introduced the co-occurrence matrix (CM) for calculation of texture contrast. It is applicable for ultrasound-normalized images:

$$\mathbf{C} = \sum_{i,j} \left| \mathbf{j-i} \right|^{k}_{d,\theta} * \mathbf{p(i,j)}^{m} \qquad \mathbf{(3)}$$

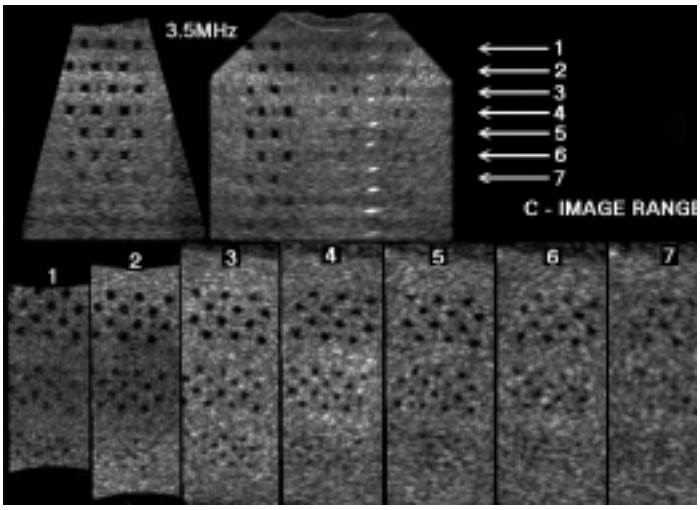


Fig. 13 - The normalization of B-images and WS processing cannot improve the detectability of small cysts. For this reason it is of serious significance to find out, for any scanner, the cyst detectability for different cyst sizes and usable scanning depths. A 3D scan shows two B-images and seven C-images of phantom with cylindrical voids from 5, 4 and 3 mm diameter in depth from 1cm to 7cm. The 3mm voids are clearly visible only at 3cm depth.

where **j** and **i** are the pixel values on distance **d** and angle **θ**. The **p(j,i)** is the probability of co-occurrence. For k=1 and m=l texture contrast definition have the best correspondence to other contrast definitions. For spherical targets and spherical reference the CR may be introduced:

$$\mathbf{CR=C/Cr} \qquad \mathbf{(4)}$$

where CR is contrast of reference. For practical test object applications, spherical or cylindrical voids are the best choice.

The inhomogeneities of a reference object could be understood also as random

distributed targets in volume. However, these targets are random in shapes and dimensions and the interpretation of contrast need some changes.

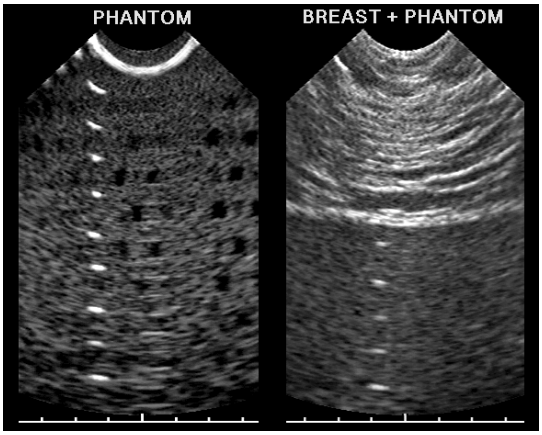


Fig. 14 - The breast when pressed, as usual in mammography, creates thee shape like “stand off” and the contrast reduction may be estimated in the same way as shown with animal fat. Only the nylon threads arc visible and the voids disappeared. The nylon threads are specular reflectors and behave obviously differently then voids.

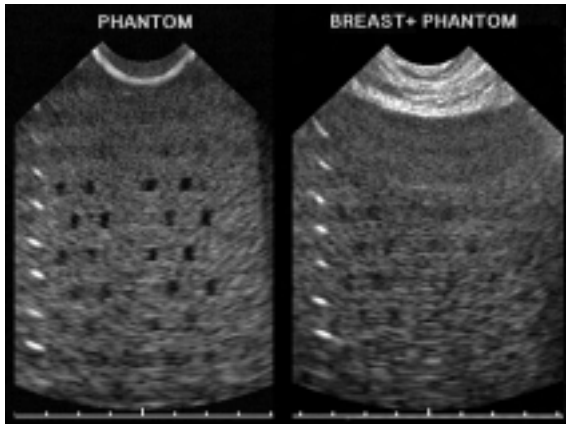


Fig. 15 - Thinner slice of breast tissue causes less contrast distortion and phantom voids are still visible.

## STATISTICAL IMAGE PROCESSING

The normalized images with a test of scanner contrast ability and a test of tissue reduction contrast, is prepared for any other speckle reduction, wavelet and fractal analysis, or any other statistical image processing. It is obvious that any other or statistical processing of the image, or part of the image, may be useless if the contrast in the region of interest (ROI) is lost or it is too much reduced. As shown, the special 3-D phantoms have to be used for measurement of contrast and contrast reduction to find out the spites of propagation in inhomogeneous media.

## CONCLUSION

The differences of ultrasound propagation in tissue and tissue mimicking materials are characterized mostly with fat interlacing of normal or pathological origin. As shown, the fat slice structures reduce the contrast essentially by inhomogenities in speed of sound and attenuation. Reverberations and multiple scattering will additionally reduce the contrast. In order to avoid the inefficient post processing of images, the contrast and contrast-reduction estimation will be suggested. The test on tissue mimicking materials is not sufficient as proof if the differences in propagation are not taken into account.

## REFERENCES

Garra, Madsen. Parks, Skelly, Zagzebski: AIUM Quality Assurance for Gray- Scale Ultrasound Scanners, Handbook (1994)

J.A. Zagzebski, Z.F. Lu, L.X. Yao: Quantitative Ultrasound imaging: in Vivo Results in Normal Liver. Ultrasonic Imaging 15, 335-351 (1993)

J. D. Satrapa: Qualitätskontrolle von ultraschall diagnostischen Geräten mit Testphantomen, Ultraschal-Diagnostik 1985, Drei-Ländertreffen, Zürich 1985
J.D. Satrapa, I. Zuna: Deterioration of B-Scan Liver Images by Abdominal Wall, The 6th WFUMB Congress, Sapporo, Japan 1994
J.C. Bamber, R.J. Dickinson: Ultrasonic B-scanning: a Computer simulation, *Phys. Med. Bio.* 1980, Vol. 25, No.3, 463-479.
D.R. Eoster, M. Arditi, F.S. Foster, M.S. Patterson, J,W.Hunt: Computer Simulations of Speckle in B-scan Images, *Ultrasonic Imaging* 5, 308-330 (1983)
J.A. Zagzebski. EL. Madsen MM. Goodsitt: Quantitative Tests of a Three-dimensional Gray scale Texture Model, *UItrasonic Imaging* 7,252-263(1985)
S. Finette: Synthetic B-scan Images by Numerical Solution of wave equation, *Ultrasound Imaging* 10, 220-228 (1988)
D.E. Robinson, L.S. Wilson, T. Bianchi: Beam pattern (Diffraction) Correction for Ultrasonic Attenuation Measurement, *Ultrasonic Imaging 6*, 293-303 (1984)
K.J. Parker, M.S.Asztely, L.M. Lerner. E.A. Schenk, R.C. Waag: In Vivo Measurements of Group and Benign Breast Diseases, *Ultrasonic Imaging* 12, 47-57, (1990)
M. Fein, I. Zuna, W.J.Lorenz: New Method of Estimating the Ultrasonic Beam Ratio Parameter for Characterizing Sound Propagation in Tissue, *Ultrasound in Med.&BioI.* Vol. 18, No.l0, pp. 881-889, 1992